The El Nino-Southern Oscillation: Relationships Between Sea Surface Temperature Anomaly, Rainfall, and Outgoing Longwave Radiation in the Central-Eastern Tropical Pacific

Benjamin Yang

The Pennsylvania State University
GEOG 417: Satellite Climatology
Professor Andrew Carleton

May 1, 2019

ABSTRACT

Reliable satellite measurements of sea surface temperature (SST), precipitation, and outgoing longwave radiation (OLR) in the central-eastern tropical Pacific are indispensable for monitoring and predicting the El Nino-Southern Oscillation (ENSO). To test the consistency of the relationships among these three variables, monthly average SST anomalies, rainfall, and OLR in the Nino 3.4 region were compared over one full ENSO cycle—April 2009 to June 2011—and linearly correlated. Datasets from the National Aeronautics and Space Administration (NASA) Earth Observations website included SST anomalies from the Advanced Microwave Scanning Radiometer - Earth Observing System (AMSR-E), OLR from the Clouds and the Earth's Radiant Energy System (CERES) sensors, and rainfall from Tropical Rainfall Measuring Mission (TRMM) Microwave Imager and Precipitation Radar. Monthly maps, 27 for each variable, were produced using the Imager Composite Explorer (ICE) analysis tool on the NASA Earth Observations website. Using Python, time series and scatter plots were created, and correlation coefficients were calculated.

The results of this investigation verified findings from past studies, clearly showing that OLR decreases as SST anomaly and rainfall increase. OLR and rainfall were strongest correlated, while SST and OLR were weakest correlated. The delayed reaction of the atmosphere to ocean warming might have explained the deepest convection that occurred one month following the highest SST anomalies during El Nino. Nonetheless, these variables were strongest correlated during El Nino and weakest correlated during La Nina, possibly due to the more spatially organized precipitation that occurred during El Nino. This investigation suggests that applying multiple variables may be advantageous in identifying the ENSO state. Future research involving more sophisticated methods, such as using different combinations of satellite instruments, study regions, and time periods, would help climatologists disseminate more accurate information regarding the ENSO on both interannual and interdecadal timescales.

INTRODUCTION

Ocean-atmosphere interactions lead to climatic variations, particularly the El Nino-Southern Oscillation (ENSO) phenomenon. The term El Nino, or "Christ Child" in Spanish, originated from fishermen off the coast of South America in the 1600s, who noticed the emergence of abnormally warm water around December (NOAA 2018). El Nino, the warming phase of sea surface temperatures (SSTs) across the central-eastern tropical Pacific, negatively impacts the Peruvian fishing industry due to the reduced upwelling of cold water. Linkages between El Nino and climate patterns around the globe, an example of teleconnections, include increased rainfall and flooding in the southern United States, a weakened east Asian winter monsoon, and reduced convergence east of Australia (Rasmusson and Carpenter 1982). On the other hand, La Nina, the cooling phase of SSTs across the central-eastern tropical Pacific, is usually linked with reduced rainfall and droughts in the southern United States. Typically, El Nino and La Nina episodes last 9-12 months and occur every 2-7 years, with La Nina events occurring more frequently, but less intensely, than El Nino events (NOAA 2018).

To accurately monitor and predict the ENSO, it is important to understand the relationships between SSTs, precipitation, and outgoing longwave radiation (OLR). During El Nino, the warmer ocean surface, thus warmer atmosphere, gives rise to deep convective clouds and precipitation. Higher sea surface temperatures are related to negative OLR anomalies. Because satellites sense the tops of clouds, they are essentially measuring cloud top temperature in the thermal infrared (TIR) range, which tends to be lower due to increased convection. The opposite takes place during La Nina—negative SSTs, positive OLR, and negative precipitation anomalies. A previous study showed that tropical Pacific SSTs and northeast Brazil precipitation are weakly correlated in January, not well correlated in February, and negatively correlated from March to May (Uvo et al. 1998). The study found that SST patterns from January to March are closely related to the precipitation from February to May, the rainy season, partly because SST anomalies exhibit 2-3-month persistence (Uvo et al. 1998). In certain regions of the central-eastern tropical Pacific, SST-OLR coupling is strong and mostly invariant with season (L'Heureux et al. 2015). As explained by Xie and Arkin (1998), correlations of around -0.6 suggest a sufficiently strong negative relationship between OLR anomalies and precipitation anomalies in the tropics on a mean annual basis. However, the precipitation observations used

were relatively low-quality, as their research was conducted before the launching of the Tropical Rainfall Measuring Mission (TRMM) satellite.

From the Northern Hemisphere (NH) spring to the end of the year, the eastern tropical Pacific SST anomaly pattern migrates from the coast of South America to around 170°W in central tropical Pacific (Rasmusson and Carpenter 1982). The National Oceanic and Atmospheric Administration (NOAA) uses the Oceanic Nino Index (ONI), which represents mean SST anomalies for the Nino 3.4 region, located at 5°N-5°S and 120°W-170°W (Golden Gate Weather Services 2019). This region is considered to be particularly sensitive to the ENSO. Despite the popularity and efficacy of the ONI in monitoring and predicting the ENSO state, some scientists have argued that the Central Pacific OLR and combined indices should be added to the current suite of ENSO indices (L'Heureux et al. 2015). A combined index of SSTs and OLR has been proven to describe more variability in winter and spring precipitation and summer temperature in North America (L'Heureux et al. 2015). Based on the Global Precipitation Climatology Project (GPCP) community precipitation dataset, with merged gauge and satellite observations, the ENSO Precipitation Index (ESPI) leads the ONI and Southern Oscillation Index (SOI) in representing the ENSO by a month (Curtis and Adler 2000). The ESPI not only produces stronger La Nina events than the ONI and SOI, but it also better describes the strength and position of the Walker circulation (Curtis and Adler 2000).

Some satellite remote sensors are active, receiving and transmitting radiation, while others are passive, only receiving radiation. All three climate variable can be measured in the TIR part of the electromagnetic spectrum, but SSTs and precipitation are also routinely detected in the microwave region. Relative to TIR images, microwave images have coarser resolution. However, where clouds exist, TIR imagery does not provide any information about the lower atmosphere or the Earth's surface. Nontraditional wavelengths, namely those in the microwave range, are advantageous because they allow for the direct sensing of precipitation through clouds. The TRMM Microwave Imager (TMI) has provided a means of collecting more quantitative data, such as rainfall rate and cloud liquid water, at lower latitudes. Henderson et al. (2018) pointed out that large discrepancies between the TMI and TRMM's Precipitation Radar (PR) in the Pacific are "related to shifts from isolated deep convection during a La Nina toward organized precipitation during El Nino." They explained that TMI rain rates increase more, in

comparison with PR rain rates, due to greater stratiform raining fractions (Henderson et al. 2018).

In addition to satellite data, conventional data from surface observing stations, ships, and buoys are used to describe the evolution of SST anomalies in the central-eastern tropical Pacific (Rasmusson and Carpenter 1982). Many satellites continuously collect data over a relatively large area of the globe, whereas conventional data are often limited in space and time. For instance, the TRMM has enabled us to monitor and study precipitation over the expansive tropical oceans. Even over land, the TRMM has helped fill in the gaps among rain gauges, which are point observations, subject to great error and bias. Aircraft lidar and doppler radar are used to provide detailed measurements of clouds and precipitation, but coverage is lacked in many parts of the world, notably remote or underdeveloped areas. The study by Henderson et. al (2018) revealed that ground validation measurements applied to TRMM rain estimates led to improved agreement between the TMI and PR. This suggests that that it is essential to incorporate both satellite and conventional data into ENSO monitoring and prediction.

To validate the satellites and results from these previous studies, this investigation seeks to address the following research questions: *1) how are satellite-derived SST anomalies, rainfall, and OLR related to one another in the central-eastern tropical Pacific? 2) to what extent are these variables correlated during an El Nino event, neutral conditions, and a La Nina event? 3) what are the limitations of satellite remote sensing for tropical ocean-atmosphere monitoring?* The time period, April 2009 to June 2011, included a moderate El Nino, neutral conditions, and a strong La Nina—one full cycle of the ENSO. Monthly average SST anomalies, rainfall, and OLR in the Nino 3.4 region were visualized on maps, plotted with time, and compared on scatter plots statistically. Based on known relationships among these three variables, OLR was expected to decrease as SST anomalies and rainfall increase over the full ENSO cycle. Furthermore, high correlation during El Nino, medium correlation during neutral conditions, and low correlation during La Nina were anticipated because clouds and precipitation tend to be more organized and consistent as SST anomalies increase. Satellite resolution, frequency, and wavelength band were expected to impact remote sensing accuracy over tropical oceans.

DATA AND METHODS OF ANALYSIS

For all three variables, datasets were obtained from the National Aeronautics and Space Administration (NASA) Earth Observations website (https://neo.sci.gsfc.nasa.gov/). This website is controlled by the Earth Observing System (EOS) Project Science Office at the NASA Goddard Space Flight Center (NEO 2019). SST anomalies were based on monthly data from the Advanced Microwave Scanning Radiometer for EOS (AMSR-E) on NASA's Aqua satellite, compared with climatological data (1985-1997) from NOAA's Advanced Very High Resolution Radiometer (AVHRR) Pathfinder satellite sensors (NEO 2019). One limitation of this data was that the AMSR-E used microwave radiation, while the AVHRR used TIR radiation (NEO 2019). Theoretically, AVHRR interpolation errors, due to the presence of clouds, canceled out over climatological timescales. Also, the 12-year climatology, although including both El Nino and La Nina years, could have been longer and extended to more recent years. The OLR data included daily, space-and-time average, top-of-the atmosphere, and surface flux observations collected by the Clouds and the Earth's Radiant Energy System (CERES) sensors on NASA's Aqua and Terra Satellites (NEO 2019). Although considered high-quality data, these daily, near-real time observations were not nearly as carefully calibrated as the standard CERES data product (NEO 2019). Rainfall amounts were derived by the TRMM Microwave Imager and Precipitation Radar instruments, with a field of view ranging from 35°N-35°S (NEO 2019). Lower resolution is related to longer wavelength; nevertheless, the TRMM has dramatically improved global precipitation measurements.

NOAA's ONI was used to determine the ENSO phase in this investigation. El Nino is declared if a five consecutive 3-month running mean of SST anomalies exceeds the threshold of +0.5°C in the Nino 3.4 region (NCDC). Accordingly, there is a La Nina when the mean is less than -0.5°C. Figure 1 outlines the Nino 3.4 region, along with several other Nino regions, which is known as an area of persistent deep convection. An approximated Nino 3.4 box (4.875°N-4.875°S, 120.125°W-169.875°W) was used in this study because of the deficiency of rounded latitude and longitude values in the datasets. As displayed in Figure 2, El Nino lasted from July 2009 to March 2010, while La Nina lasted from June 2010 to May 2011. Neutral conditions occurred on April-June 2009, April-May 2010, and June 2011. An El Nino or La Nina event is considered weak if the magnitude of the ONI is between 0.5 and 0.9, moderate if between 1.0

and 1.4, strong if between 1.5 and 1.9, and very strong if greater than 2.0 (Golden Gate Weather Services 2019). Notwithstanding, the 2009-10 El Nino was classified as moderate, even though the magnitude of the ONI was practically the same as that of the strong 2010-11 La Nina.

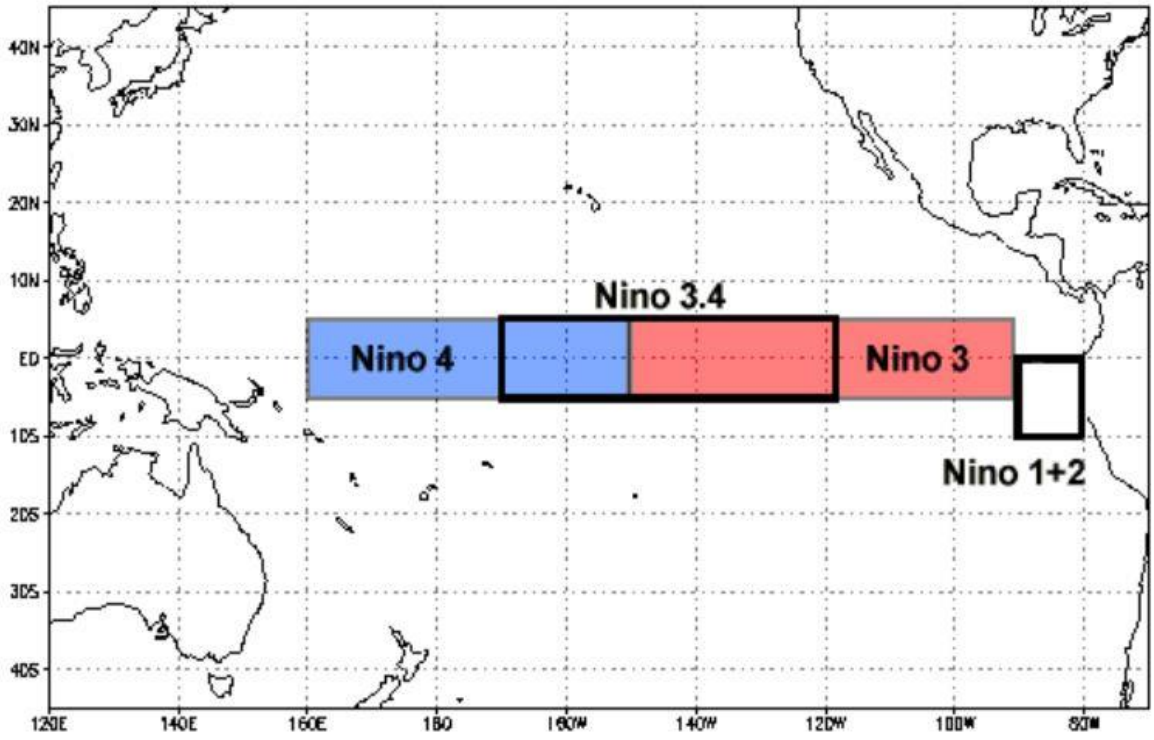

Figure 1. The various Nino regions for the tropical Pacific. Nino 3.4 (5°N-5°S, 120°W-170°W) was used for this investigation. *Source: https://www.ncdc.noaa.gov/teleconnections/enso/indicators/sst/.*

2009	**-0.8**	**-0.7**	**-0.5**	-0.2	0.1	0.4	**0.5**	**0.5**	**0.7**	**1.0**	**1.3**	**1.6**
Year	**DJF**	**JFM**	**FMA**	**MAM**	**AMJ**	**MJJ**	**JJA**	**JAS**	**ASO**	**SON**	**OND**	**NDJ**
2010	**1.5**	**1.3**	**0.9**	0.4	-0.1	**-0.6**	**-1.0**	**-1.4**	**-1.6**	**-1.7**	**-1.7**	**-1.6**
2011	**-1.4**	**-1.1**	**-0.8**	**-0.6**	**-0.5**	-0.4	**-0.5**	**-0.7**	**-0.9**	**-1.1**	**-1.1**	**-1.0**

Figure 2. Running 3-month mean ONI values. Red indicates the El Nino phase, black indicates the neutral phase, and blue indicates the La Nina phase. Note the time period April 2009 to June 2011. *Source: https://origin.cpc.ncep.noaa.gov/products/analysis_monitoring/ensostuff/ONI_v5.php.*

Using the Image Composite Explorer (ICE) analysis tool on the NASA Earth Observations website, monthly SST anomaly, rainfall, and OLR maps were produced. For each of the 27 months, the latitudes and longitudes of the Nino 3.4 box, "Basic Exploration" mode, and "0.25 degrees" file size were inputted before launching the analysis. Since there was no simple way of downloading all the maps at once, screenshots were manually taken and combined into a single figure for each variable. Hence, the map areas may have varied slightly. The overall patterns within the Nino 3.4 region were negligibly affected. As described on ICE analysis tool page, the data values were based upon the scaled range of the imagery, and, thus, this technique should not be employed in more extensive research endeavors (NEO 2019).

The monthly datasets were downloaded as "CSV for Excel" files, each with 1440 x 720 dimensions and values spaced 0.25 degrees apart. For efficiency, a Python program was designed and run to read each file for each variable. The mean of the two-dimensional array of Nino 3.4 values was calculated each time, resulting in 27 mean values for each variable. Using these mean values, a time series plot of SST anomaly, rainfall, and OLR was created to show how these variables were related in different months. Next, three scatter plots—SST anomaly versus rainfall, SST anomaly versus OLR, and OLR versus rainfall—were produced to show the relationships among the variables. Linear regression was performed on all values in each correlation. Additionally, correlation coefficients (r) for each relationship were calculated, which can be found by hand using the formula

$$r = \frac{\sum(x - \bar{x})(y - \bar{y})}{\sqrt{\sum(x - \bar{x})^2}\sqrt{\sum(y - \bar{y})^2}} \qquad (1)$$

where x is the independent variable and y is the dependent variable. Knowing the dates of the El Nino, neutral, and La Nina events, the correlation coefficients for each ENSO phase, nine in total, were computed.

RESULTS AND DISCUSSION

As presented in Figure 3, most of the SST anomalies in the central-eastern tropical Pacific were near zero in April 2009, becoming increasingly positive throughout the year. The peak in SST anomalies occurred around January 2010, which was when ONI values were maximum. Negative SST anomalies began to show up again during the transition into La Nina, reaching the lowest values around November 2010, which was when ONI values were minimum. SST anomalies became less negative as the La Nina weakened and transitioned into neutral conditions. In the western portion of the domain, the SST anomalies varied the most from El Nino to La Nina, suggesting that this area is more sensitive to the ENSO. The higher SST anomalies seem to have moved from east to west as the El Nino strengthened, while the lower SST anomalies seem to have moved from west to east as the La Nina strengthened. This likely signifies the presence of Kelvin and Rossby waves, which propagate over the tropical Pacific.

Figure 4 shows monthly rainfall, which followed somewhat different patterns than those of SST anomalies over the central-eastern tropical Pacific. It appears that rainfall slightly decreased during 2009, particularly in the NH early fall. Rainfall reached the highest values in February 2010, but were more consistently high across the domain in April 2010. As Uvo et al. (1998) described, SST anomalies exhibit 2-3-month persistence, which may be less in the Nino 3.4 region. These results were potentially due to the delayed response of the atmosphere to increasing ENSO SST anomalies. Rainfall decreased throughout the rest of 2010, reaching minimum values around or a little after November 2010, when ONI values were minimum. However, rainfall noticeably increased in the NH late winter and early spring. This may be because many of the SST anomalies were still above the threshold for persistent deep convection to occur, despite negative SST anomalies in this region (NCDC).

Although negatively related to rainfall, OLR was quite comparable to rainfall spatially and temporally, as depicted in Figure 5. OLR increased slightly during the NH late summer and early fall. The minimum OLR values appeared around February 2010, notably in the western portion of the domain. As El Nino weakened and La Nina strengthened, OLR values increased. In the NH late winter and early spring 2011, the OLR values decreased, although not nearly as much as some of the OLR values during the El Nino. These maps imply a strong relationship between OLR and rainfall, which is explicitly shown in Figure 9.

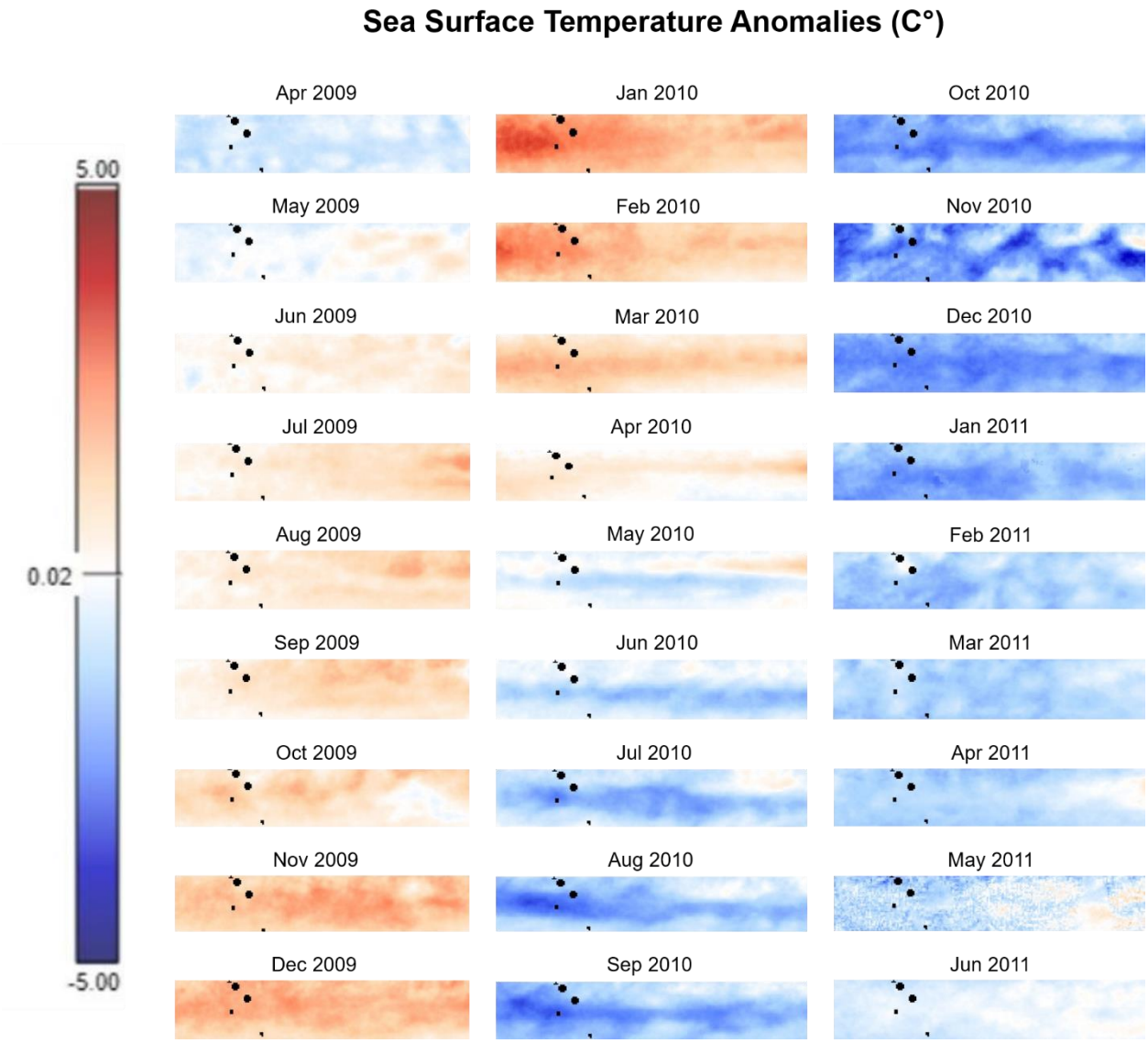

Figure 3. Monthly maps of SST anomalies in the Nino 3.4 region from April 2009 to June 2011. Warmer colors indicate positive SST anomalies, while cooler colors indicate negative SST anomalies. Black represents areas with no available data (i.e. land). *Source: https://neo.sci.gsfc.nasa.gov/.*

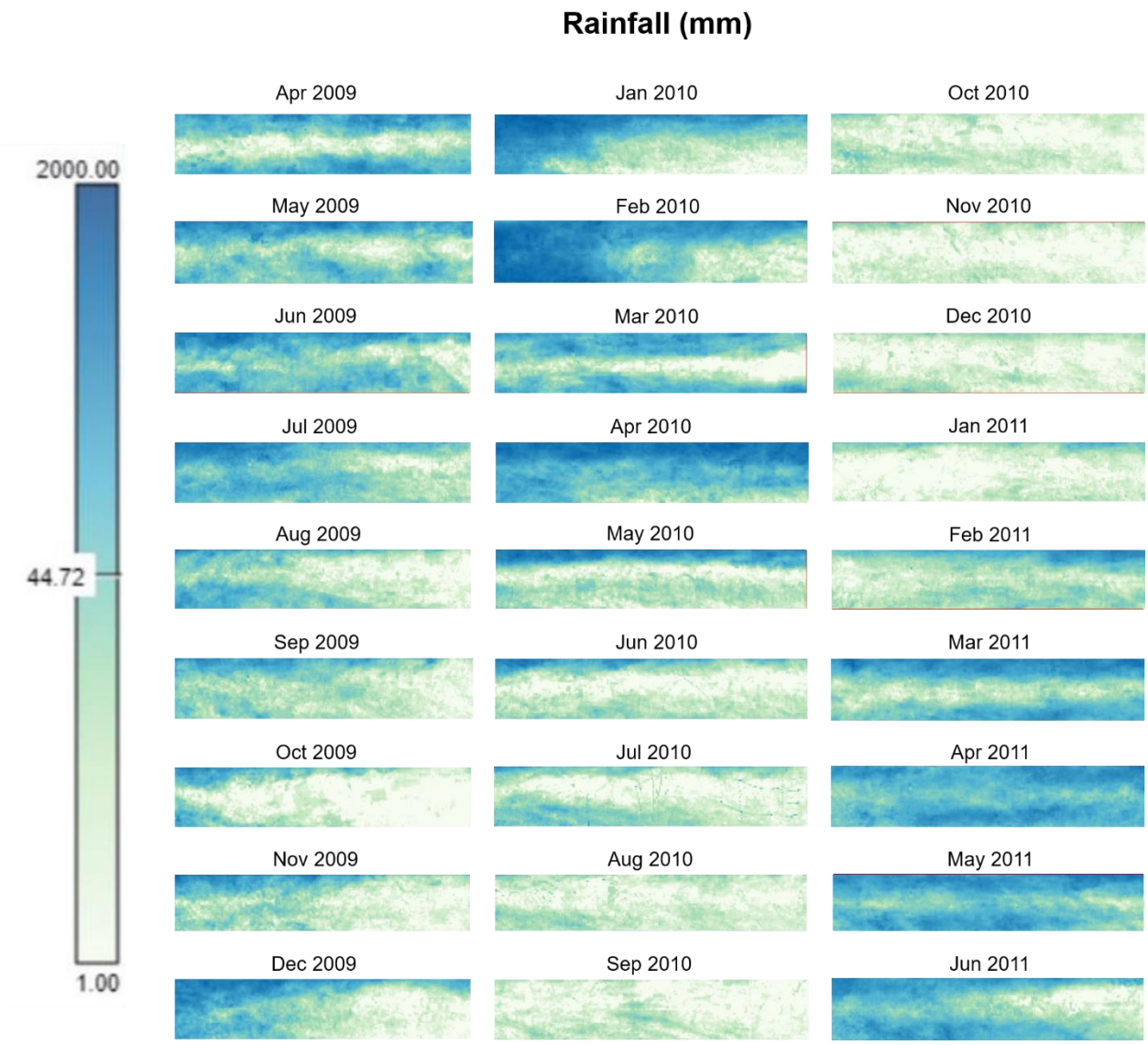

Figure 4. Monthly maps of rainfall in the Nino 3.4 region from April 2009 to June 2011. Darker colors indicate higher rainfall, while lighter colors indicate lower rainfall. *Source: https://neo.sci.gsfc.nasa.gov/.*

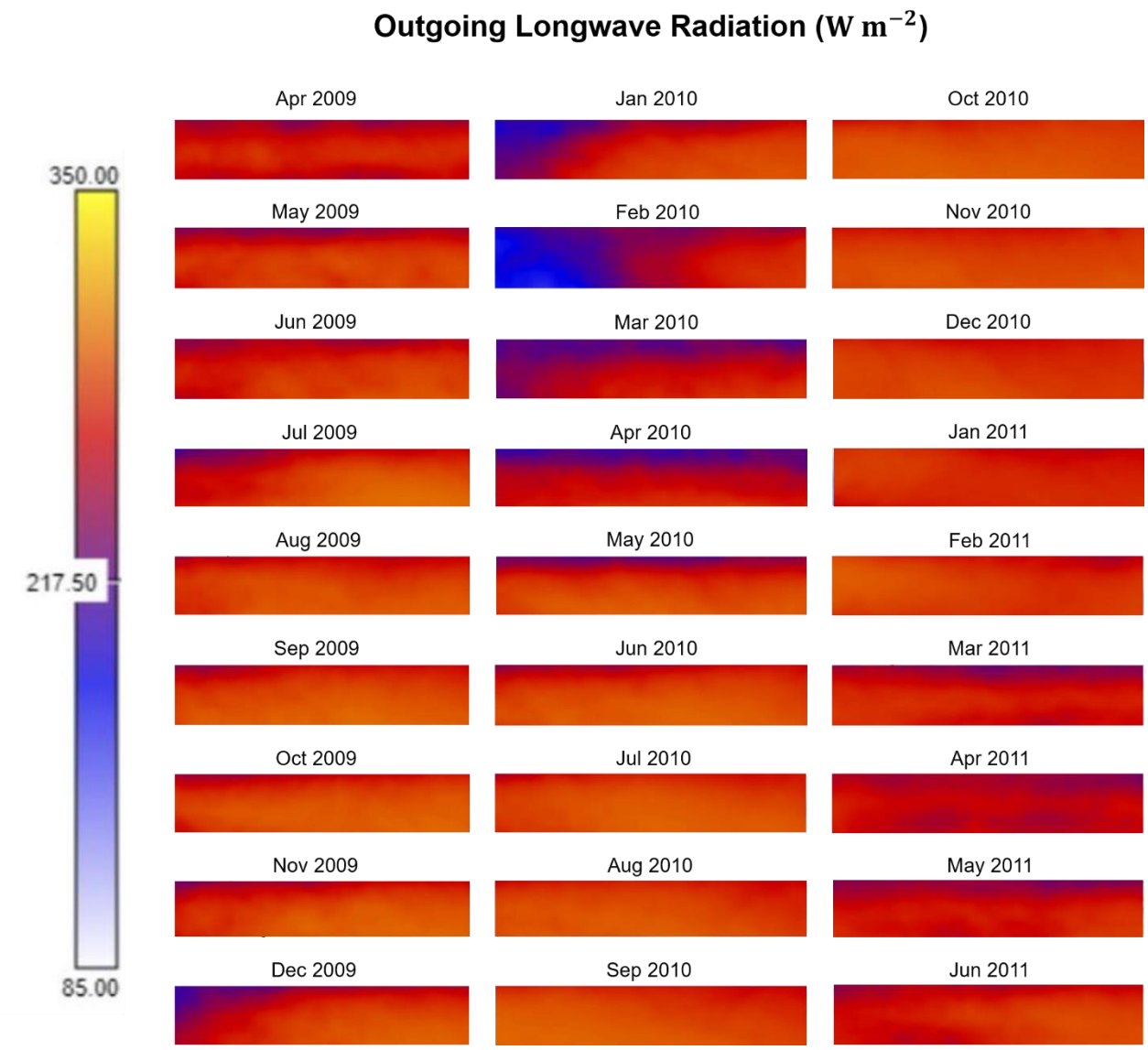

Figure 5. Monthly maps of OLR in the Nino 3.4 region from April 2009 to June 2011. Orange indicates greater OLR, while blue indicates less OLR. *Source: https://neo.sci.gsfc.nasa.gov/.*

In Figure 6, the temporal variations in mean SST anomaly, rainfall, and OLR and relationships among these variables are illustrated. SST anomaly increased throughout 2009, reached its maximum around January 2010, decreased throughout 2010, reached its minimum around December 2010, and increased thereafter. These trends are similar to those displayed in Figure 3. OLR values were relatively high in NH late summer and early fall 2009 and then again in mid-late 2010. The minimum OLR value occurred on February 2010, with a smaller decrease in OLR around April 2011. As the direct opposite of OLR, rainfall generally increased when OLR decreased and decreased when OLR increased. January to February 2011 was the exception, when both OLR and rainfall increased. This might suggest that lower clouds did not always have higher temperatures or produce less rainfall due to other factors, suggest as advection by winds. Although these three variables seem to have been well correlated, the response to the highest SST anomalies was slightly delayed, as evident in the separation between SST anomaly and OLR maxima by one month.

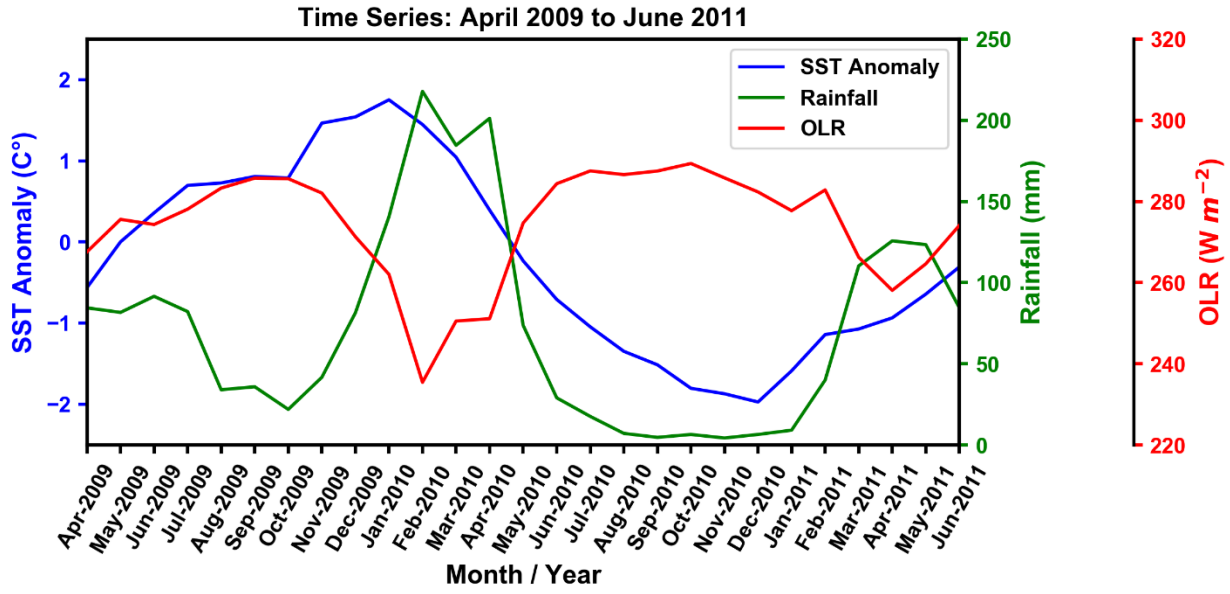

Figure 6. Time series plot of mean SST anomaly (blue), rainfall (green), and OLR (red) in the Nino 3.4 region from April 2009 to June 2011. *Data: https://neo.sci.gsfc.nasa.gov/.*

The correlation coefficients indicate that OLR and rainfall were strongest correlated (Figure 9), SST anomaly and rainfall were weaker correlated (Figure 7), and SST anomaly and OLR were weakest correlated. Nevertheless, the overall relationships among the variables were validated—a positive relationship between SST anomaly and rainfall, a negative relationship between SST and OLR, and a positive relationship between OLR and rainfall. The strong correlation between OLR and rainfall is consistent with the findings of Xie and Arkin (1998). Unlike the strong SST-OLR coupling noted by L'Heureux et al. (2015), the correlation between SST anomaly and OLR was weakest. However, a correlation coefficient of -0.44, displayed in Figure 8, is still considerable. The weaker correlations (Figure 7 and Figure 8) might have been due to inconsistencies in SST anomaly measurements, which could partially have been due to AMSR-E relying on a different wavelength range (microwave) than that of the AVHRR (TIR). For distinct ENSO phases, the correlation coefficients for SST anomaly versus rainfall are roughly the same, with a slightly stronger correlation during neutral conditions. SST anomaly and OLR clearly had the strongest correlation during an El Nino, while there were similar correlations during the neutral and La Nina phases. OLR and rainfall were strongest correlated during El Nino and weakest correlated during La Nina. Considering all three scatter plots, the variables had the strongest relationships during El Nino and weakest relationships during La Nina. More organized precipitation during El Nino, as Henderson et al. (2018) mentioned, allowing the satellite to more accurately sense large-scale patterns, likely explained the stronger relationships among these variables.

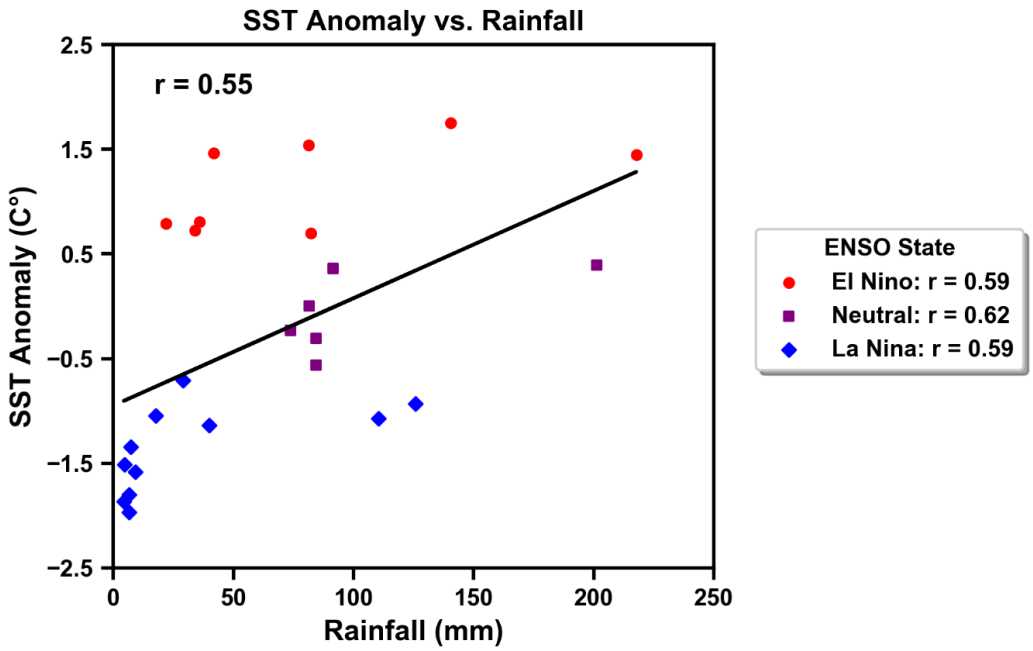

Figure 7. Linear correlation between mean SST anomaly and rainfall. The best fit line and correlation coefficient are displayed. El Nino (red circles), neutral (purple squares), and La Nina (blue diamonds) are differentiated, with their correlation coefficients shown in the legend. *Data: https://neo.sci.gsfc.nasa.gov/.*

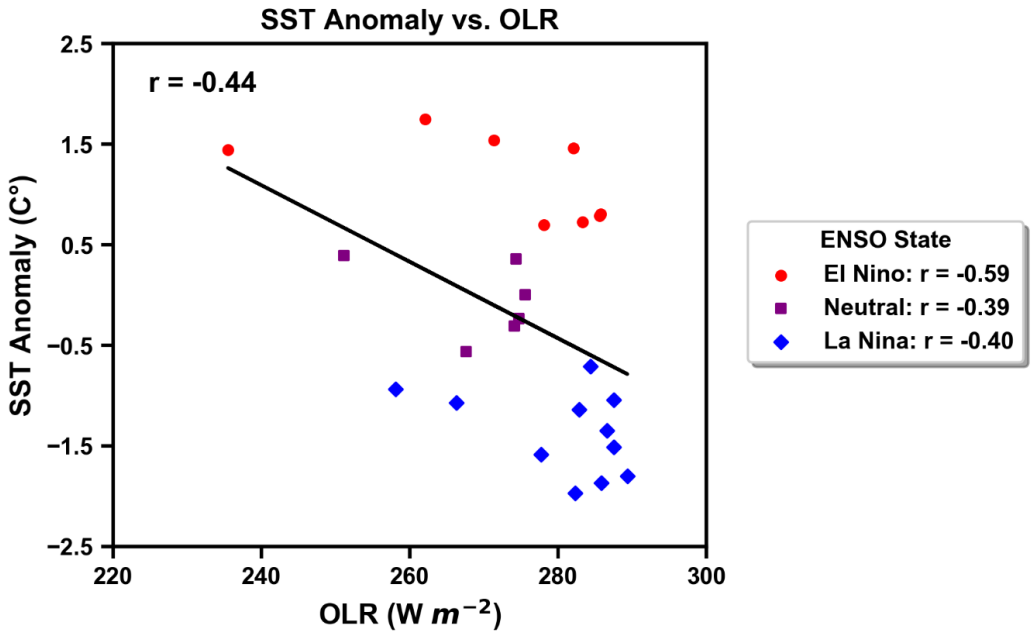

Figure 8. Linear correlation between mean SST anomaly and OLR. The best fit line and correlation coefficient are displayed. El Nino (red circles), neutral (purple squares), and La Nina (blue diamonds) are differentiated, with their correlation coefficients shown in the legend. *Data: https://neo.sci.gsfc.nasa.gov/.*

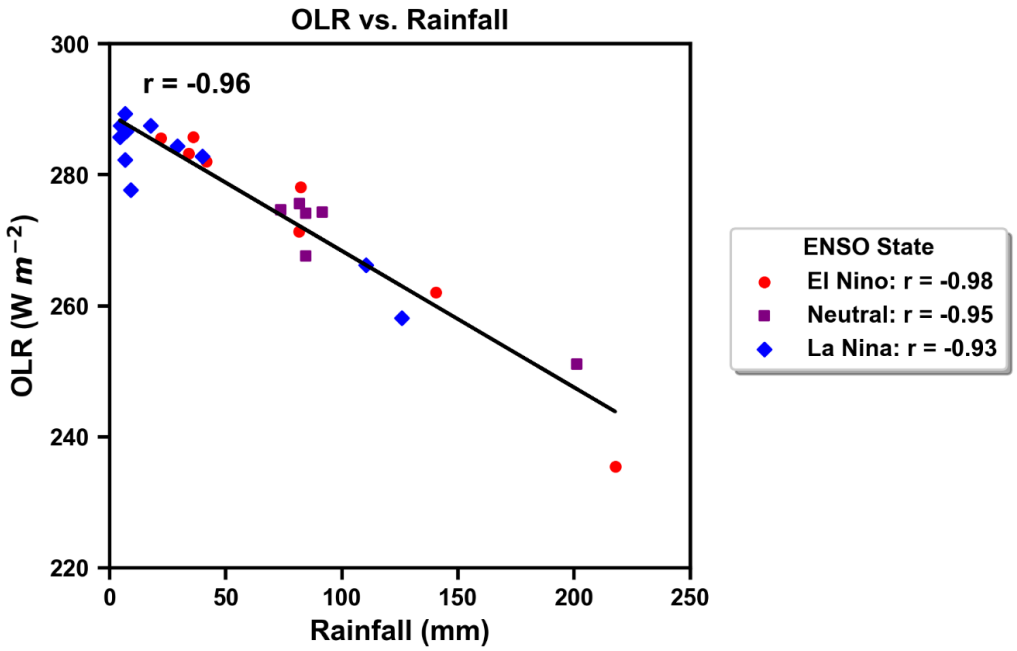

Figure 9. Linear correlation between mean OLR and rainfall. The best fit line and correlation coefficient are displayed. El Nino (red circles), neutral (purple squares), and La Nina (blue diamonds) are differentiated, with their correlation coefficients shown in the legend. *Data: https://neo.sci.gsfc.nasa.gov/.*

SUMMARY AND CONCLUSIONS

The primary objectives of this investigation were to assess the relationships between SST anomalies, rainfall, and OLR, determine the correlations among these variables during different ENSO phases, and identify the limitations of satellite remote sensing of the ENSO. While most previous studies agree that, in general, there are strong correlations among these variables, some studies showed that these correlations can significantly vary depending on the study region, time of year, and type of satellite sensor. To validate these findings and test the hypothesis that correlations are highest during El Nino and lowest during La Nina, monthly average SST anomalies, rainfall, and OLR in the Nino 3.4 region were evaluated and compared with one another over one full ENSO cycle. The satellite observations used in this study included AMSR-E microwave-derived SST anomalies, CERES infrared-derived OLR, and TRMM microwave and radar-derived rainfall. Maps were produced using NASA's ICE analysis tool, while time series and scatter plots were produced in Python. Correlation coefficients were not only found for each variable throughout the entire period, but also for El Nino, neutral, and La Nina events, separately.

As expected, SST anomalies and rainfall increased during El Nino development and decreased during La Nina development. However, the peak in rainfall followed the highest SST anomalies one month later, suggesting that the atmosphere had a delayed response to the ocean. Similarly, OLR reached minimum values one month after the highest SST anomalies. Overall, the known relationships between SST anomalies, rainfall, and OLR over time were confirmed, with the exception of January to February 2011. All figures of OLR versus rainfall showed that these two variables were strongest correlated, whereas figures of SST anomaly versus OLR revealed that these two variables were weakest correlated. Despite the inconsistencies in the correlation coefficients, the variables seemed to be have been strongest correlated during an El Nino, perhaps because of the more spatially organized precipitation, compared with more isolated convective cells during neutral or La Nina conditions.

These results suggest that multiple variables can be used in identifying the ENSO state. Although the ONI is widely considered the default ENSO index, a combined index of SST, rainfall, and OLR—or any pair of these variables—may aid in more accurately monitoring and predicting the ENSO. Furthermore, this investigation demonstrates that it is acceptable to use

both direct and indirect methods of satellite remote sensing to analyze the ENSO. Microwave sensors are capable of sensing precipitation through clouds, while TIR sensors lead to finer resolution images. Future studies are needed to validate these results, using different combinations of time periods, satellite instruments, and perhaps ground truth measurements. Moreover, one should not be limited to the Nino 3.4 region; other areas of the central-eastern tropical Pacific are also quite sensitive to the ENSO. Ideally, one would incorporate datasets with rainfall anomalies and OLR anomalies, comparing these with SST anomalies. These studies would further add to our understanding of the ENSO, which affects people around the globe on an interannual timescale and, conceivably, on longer timescales increasingly due to climate change.

REFERENCES

Curtis, S., and R. Adler, 2000: ENSO Indices Based on Patterns of Satellite-Derived Precipitation. *Journal of Climate*, **13**, 2786–2793, doi:10.1175/1520-0442(2000)013<2786:eibopo>2.0.co;2.

Golden Gate Weather Services, 2019: El Nino and La Nina Years and Intensities. *Golden Gate Weather Services*. https://ggweather.com/enso/oni.htm (Accessed May 1, 2019).

Henderson, D. S., C. D. Kummerow, and W. Berg, 2018: ENSO Influence on TRMM Tropical Oceanic Precipitation Characteristics and Rain Rates. *Journal of Climate*, **31**, 3979–3998, doi:10.1175/jcli-d-17-0276.1.

L'Heureux, M. L., M. K. Tippett, and A. G. Barnston, 2015: Characterizing ENSO Coupled Variability and Its Impact on North American Seasonal Precipitation and Temperature. *Journal of Climate*, **28**, 4231–4245, doi:10.1175/jcli-d-14-00508.1.

NCDC, Equatorial Pacific Sea Surface Temperatures. *National Climatic Data Center*. https://www.ncdc.noaa.gov/teleconnections/enso/indicators/sst/ (Accessed May 1, 2019).

NEO, NASA Earth Observations. NASA. https://neo.sci.gsfc.nasa.gov/ (Accessed May 1, 2019).

NOAA, 2018: What are El Nino and La Nina? *NOAA's National Ocean Service*. https://oceanservice.noaa.gov/facts/ninonina.html (Accessed May 1, 2019).

NOAA, 2019: Cold & Warm Episodes by Season. *Climate Prediction Center*. https://origin.cpc.ncep.noaa.gov/products/analysis_monitoring/ensostuff/ONI_v5.php (Accessed May 1, 2019).

Rasmusson, E. M., and T. H. Carpenter, 1982: Variations in Tropical Sea Surface Temperature and Surface Wind Fields Associated with the Southern Oscillation/El Niño. *Monthly Weather Review*, **110**, 354–384, doi:10.1175/1520-0493(1982)110<0354:vitsst>2.0.co;2.

Uvo, C. B., C. A. Repelli, S. E. Zebiak, and Y. Kushnir, 1998: The Relationships between Tropical Pacific and Atlantic SST and Northeast Brazil Monthly Precipitation. *Journal of Climate*, **11**, 551–562, doi:10.1175/1520-0442(1998)011<0551:trbtpa>2.0.co;2.

Xie, P., and P. A. Arkin, 1998: Global Monthly Precipitation Estimates from Satellite-Observed Outgoing Longwave Radiation. *Journal of Climate*, **11**, 137–164, doi:10.1175/1520-0442(1998)011<0137:gmpefs>2.0.co;2.